THE ASTROPHYSICAL JOURNAL, 423:621–632, 1994 March 10


# THE COMPLEX SOFT X-RAY EXCESS IN NGC 4151

K. A. WEAVER,[1,2] R. F. MUSHOTZKY, K. A. ARNAUD,[1] P. J. SERLEMITSOS, F. E. MARSHALL,
R. PETRE, K. M. JAHODA, AND A. P. SMALE[3]
NASA/Goddard Space Flight Center, Greenbelt, MD 20771

AND

H. NETZER
School of Physics and Astronomy and the Wise Observatory, Tel Aviv University, Tel Aviv 69978, Israel
*Received 1993 June 15; accepted 1993 September 21*

## ABSTRACT

We present Broad-Band X-ray Telescope (BBXRT) observations (~0.4–11.0 keV) of the Seyfert 1.5 galaxy NGC 4151, with emphasis placed upon modeling the low-energy X-ray spectrum. A prominent soft X-ray "excess" below the ~2 keV cutoff due to a high absorbing column is known to exist in NGC 4151. This excess has been variously discussed in terms of "leakage" through a patchy absorber, the reduced opacity of an ionized absorber, and/or a distinct and possibly spatially extended component. BBXRT, with its combination of moderate resolution and a large bandpass, has allowed the origin of this excess to be tested for the first time over a 2 day period. We find that the ~0.4–1.5 keV flux remains essentially constant while the 2–10 keV continuum flux decreases by ~40%. We also see no evidence of strong spectral features at energies of less than 1.5 keV. This implies that the excess is neither continuum "leakage" nor is it dominated by emission from a $10^6$–$10^7$ K equilibrium plasma. The best single-component description of the soft excess is scattering of the central continuum into our line of sight by an "electron scattering zone" similar to that in the Seyfert 2 galaxy NGC 1068. However, a more likely description of the lack of strong spectral features and the lack of correlated soft-to-hard X-ray variability is that at least two spectral components comprise the soft excess.

*Subject headings:* galaxies: individual (NGC 4151) — galaxies: nuclei — galaxies: Seyfert — X-rays: galaxies

## 1. INTRODUCTION

NGC 4151 is a nearby ($D = 20$ Mpc for $H_0 = 50$), barred spiral galaxy viewed almost face-on (Simkin 1975; Pedlar et al. 1992) containing a Seyfert 1 type active nucleus (Khachikian & Weedman 1974). Besides being one of the nearest it is also one of the intrinsically weakest Seyfert galaxies at X-ray energies, having $L_{X(2-10)} \sim 7 \times 10^{42}$ ergs s$^{-1}$. Because of its proximity, NGC 4151 is perhaps the best known and studied Seyfert galaxy at all wavelengths.

NGC 4151 was first identified as an X-ray source by Gursky et al. (1971) and has been detected out to energies of at least 500 keV (Perotti et al. 1981). The 2–10 keV X-ray continuum flux typically exhibits a slow drifting behavior (in contrast to showing flarelike events) with a minimum doubling timescale of ~0.5 days. There is evidence for a flux-spectral index correlation (Perola et al. 1986; Yaqoob & Warwick 1991; Yaqoob et al. 1993) that may hold down to timescales of hours. There is also evidence that the variability of the optical-UV and X-ray continua are well correlated (Perola et al. 1986).

NGC 4151 exhibits a complex and continually changing spectral shape. Its ~2–10 keV spectrum consists of an absorbed power law with a variable photon index, ranging from 1.35–1.7 (Yaqoob & Warwick 1991) and a strong, narrow 6.4 keV Fe K$\alpha$ emission feature (Weaver et al. 1992, hereafter Paper I). The measured X-ray column density ranges from $3\text{–}15 \times 10^{22}$ cm$^{-2}$ and appears to be variable on timescales of months to years (Barr et al. 1977; Yaqoob, Warwick, & Pounds 1989; Yaqoob et al. 1993). Below ~3 keV, a prominent excess of soft photons is observed above an extrapolation of a uniformly absorbed power law to lower energies. This "primary" soft excess was discovered by Holt et al. (1980) and is generally modeled by allowing some fraction (typically 10%) of the central source to be completely uncovered or viewed through a lower column (the so-called "partial covering" or "leaky absorber" model). In addition, there is evidence of a possibly separate soft excess component that does not vary with the 2–10 keV continuum (Pounds et al. 1986; Perola et al. 1986).

Extended soft X-rays, which make up ~15% of the 0.1–3.0 keV flux, have been found to the SW of the nucleus (Elvis, Briel, & Henry 1983). These X-rays appear to be associated with the emission-line gas that extends asymmetrically also to the SW of the nucleus (Heckman & Balick 1983), with a total extent of 30″–40″ (Peréz-Fournon & Wilson 1990). It is not yet clear how the resolved extended component is associated with the soft excess seen in the spectral data, but the flux in the extent appears to make up less than 30% of the total soft excess between 0.1–3.0 keV (Elvis et al. 1983; Perola et al. 1986).

Although the general aspects of the shape of the X-ray continuum are well determined, quite a large disagreement on the "specifics" of the spectral shape exists in the literature. First, the energy of the observed onset of the primary (partial covering) soft excess changes, ranging from 2 keV (Holt et al. 1980) to almost 4 keV (Perola et al. 1986; Warwick et al. 1989; Yaqoob & Warwick 1991). Second, the spectrum of the nonvariable soft component is also uncertain, and values of $kT$ from 0.15 to 0.58 keV for a thermal bremsstrahlung model have been observed (Perola et al. 1986; Pounds et al. 1986). Some discrepancies can be attributed to the very low energy

[1] Also University of Maryland.
[2] Presently at the Department of Astronomy and Astrophysics, 525 Davey Lab, Pennsylvania State University, University Park, PA 16802.
[3] With the Universities Space Research Association.

resolution of proportional counter experiments; however, it may be that different components dominate at different epochs.

In this paper, we present new soft X-ray spectral data on NGC 4151. We report a selected subset of the BBXRT observations and discuss background subtraction and spectral analysis in § 2. In § 3 we compare the new data with various model predictions and present a partial reanalysis of *Einstein Observatory* SSS and MPC data in light of the BBXRT results. The implications of the BBXRT results are discussed in § 4, and the conclusions are stated in § 5.

## 2. OBSERVATIONS AND DATA ANALYSIS

The Broad-Band X-ray Telescope, which flew successfully on the space shuttle Columbia as part of the Astro-1 mission in 1990 December, consists of two identical telescopes (designated A and B) with light-weight nested foil mirrors to focus X-rays onto two segmented (five element or "pixel") solid state detectors. The field of view of each central detector element (A0 or B0) is 4′ in diameter, and the total field of view including the outer pixels is 17′. A 1′ mask is located between the central and outer detector elements. BBXRT covers a bandpass of 0.3–12 keV. This offers improvement over proportional counters and previous solid-state detectors in that both the soft- and medium-energy X-ray regimes are covered simultaneously. A full discussion of the instrument and calibration can be found in Serlemitsos et al. (1992) and Weaver et al. (1994).

Figure 1 illustrates the A detector pixels superposed on an *Einstein Observatory* IPC image of NGC 4151. This represents the orientation of the A telescope when NGC 4151 was observed ~1.′5 off-axis during the final pointing on day 6 of the mission. The outer A pixels are labeled A1–A4 in a direction on the sky that is counter-clockwise, while the B detector (not shown) is rotated by 180° with respect to A such that A1 and B3 observe the same area of the sky. There is also a slight offset between the A and B telescopes. The mean displacement of B with respect to A is 0.′82 at an azimuth of 117°. This azimuth is measured from the radial line that separates the A2/A1 boundary (Fig. 1) and represents a 117° rotation through A1 toward A4. In other words, for a source on-axis in A0, the distribution of counts in the outer B pixels will be maximized in B4 (which is the A2 counterpart). Since the A system axis was used as the nominal pointing position of the telescope, the count rates reported here are A rates. In this paper, the term "on-axis" refers to a source that is centered in the A detector.

The source seen in pixel A1 in Figure 1 is a known soft X-ray source located ~5′ to the NW of NGC 4151 which has been identified as the BL Lacertae object 1208+39 (R.A. $12^h7^m55^s$ Decl. +39°46′1″). When NGC 4151 is approximately centered in the detector, the two objects are spatially resolved and the BL Lac object contributes less than 1.0% of the flux between 0.5–1.5 keV. However, when NGC 4151 is observed in an outer

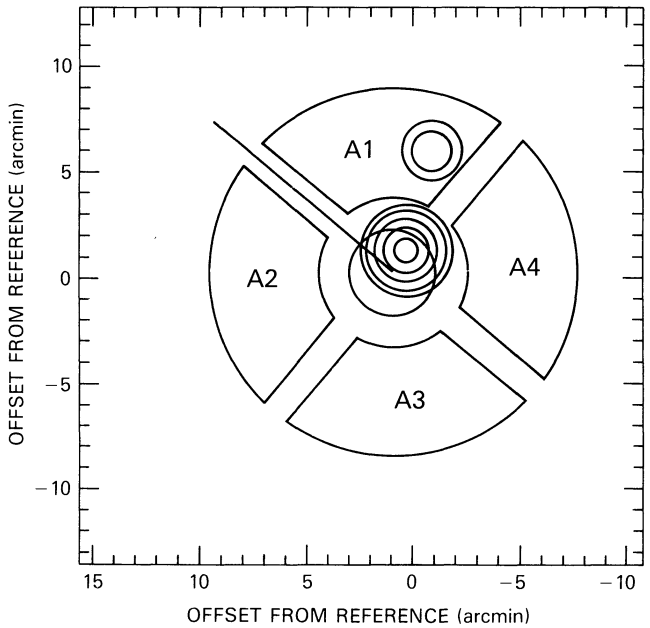


FIG. 1.—The BBXRT A-detector pixels superposed on an *Einstein* IPC image of the NGC 4151 field. North is up, and east is to the left. Identified X-ray sources are NGC 4151 (in the central pixel) and the BL Lac 1208+39 to the NW. Contour levels are 8%, 15%, 30%, 50%, and 80% of the peak flux.

pixel, ~30% of the total counts between 0.5–1.5 keV are contributed by the BL Lac object. In order to avoid contamination by the BL Lac object when modeling the form of the soft X-ray spectrum, we restrict ourselves to the approximately on-axis observations only. Of the six NGC 4151 observations, only two met this criterion (Table 1). For the data presented in this paper, the positions of the source in A detector coordinates are 0′ and 1.′5 off-axis.

Both of the approximately on-axis observations were obtained during orbit day when Thompson- and fluorescently scattered solar radiation from Earth's atmosphere contributes most of the low-energy background. The intensity of this scattered radiation varies with the Earth angle, defined as the angle between the pointing direction of the telescope and Earth's center. At no time during either observation was the Earth angle much less than 90°, so the only major daytime background is the oxygen fluorescence line at 0.524 keV (Weaver et al. 1994). During the NGC 4151 observations, the oxygen feature contributes 50% of the observed flux in a 128 eV wide energy bin at ~0.5 keV.

The non–X-ray detector background count rate at medium (2–10 keV) energies is found to scale linearly with the detector guard rate, a housekeeping parameter that indicates the rate of particle interactions with a plastic scintillator surrounding

TABLE 1

SELECTED OBSERVATIONS OF NGC 4151

| Observation | MET[a] (decimal day) | Duration (s) | Off-Axis | 2–10 keV count rate (counts $s^{-1}$) | 0.5–1.5 keV count rate (counts $s^{-1}$) |
|---|---|---|---|---|---|
| 1..... | 5.927 | 1150.2 | 0.′0 | 3.91 ± 0.06 | 0.23 ± 0.02 |
| 2..... | 6.622 | 1555.2 | 1.5 | 2.40 ± 0.04 | 0.21 ± 0.02 |

NOTE.—Count rate is vignetting-corrected for A0 and B0 pixels combined.

[a] $0^h$ MET is 1990 day 336 $06^h49^m01^s$ UT.

most of the detector (Jahoda et al. 1992; Weaver et al. 1994). This linear relation of the non–X-ray background count rate to the guard rate can be extrapolated to low energies (<2 keV) as well. During the NGC 4151 observations the non–X-ray background contributes ~1% of the observed flux at 0.5 keV.

Background subtraction was performed by first accumulating data from off-source observations during "orbit day" for the same range of Earth angles as the source observation. This produced a predicted background spectrum containing scattered X-rays as well as the contribution from the diffuse X-ray background. The non–X-ray detector background was then subtracted from this spectrum and replaced with non–X-ray background that had been scaled to match the count rate predicted by the guard rate measured during the NGC 4151 observation. For observations of weak point sources on-axis, the BBXRT outer pixel data provide a direct estimate of the simultaneous background. Each central pixel background spectrum was verified to be correct by comparing its associated outer pixel counterpart to outer pixel data obtained during the NGC 4151 observation. The background files used for the data analysis left no significant positive or negative residuals when subtracted from the data in an outer "off-source" pixel.

For each observation, the background subtracted A0 and B0 pixel pulse-height data files were fit simultaneously using the XSPEC spectral fitting package (Shafer, Haberl, & Arnaud 1989) with appropriate detector response matrices. BBXRT has a total of 512 pulse-height channels. The first 15 of these, below the lower level discriminator threshold, are unusable and were ignored in the spectral fitting. Channel 512 is an overscale channel and was also ignored in the spectral fitting. The remaining channels were "grouped" to have eight resolution elements per bin which gave roughly ≥20 counts in each bin. This allowed the use of chi-square statistics for spectral fitting. In all of the fits presented, the data were modeled ignoring grouped bins 16 and 74–78 because there were significantly fewer than 20 counts in those bins. A total of 57 grouped bins in each spectrum covering 0.4–11.0 keV were used in the fitting procedure.

To reduce the number of free parameters, the normalizations of each model component were tied together between the A0 and B0 data files during fitting. This allowed only one normalization per model component to vary. Based on the aspect solution, the B0 normalizations for each model component were set to 0.96 and 1.04 times the A0 normalizations for days 5 and 6, respectively. The B0 normalization is slightly higher with respect to the A normalization on day 6 because of the telescope offset (i.e., the source is more "on-axis" in B). All of the fits discussed in this paper also include a narrow Fe Kα line with an energy fixed at 6.38 keV. This is the expected energy for redshifted cold iron ($z = 0.0033$) and is consistent with the measured energy for the narrow line in the unbinned data (6.35 ± 0.03 keV; Paper I).

## 3. RESULTS

### 3.1. *Variability*

The 0.5–1.5 and 2–10 keV vignetting-corrected, background-subtracted source count rates for the A0 and B0 pixels combined are given in Table 1. The 0.5–1.5 keV count rate remains constant while the 2–10 keV source count rate is observed to decrease by ~40% over a period of 17 hr. Throughout the rest of the paper, we will refer to the day 5 observation as the "high" flux state of the source and the day 6 observation the "low" flux state.

### 3.2. *Spectrum*

The 0.4–11.0 keV data were initially fitted with a model consisting of an Fe Kα line and a power-law continuum [the photon index Γ is defined as $N(E) \propto E^{-\Gamma}$] suffering low-energy absorption by a uniform column of cold gas. This gave an unacceptable fit, resulting in reduced $\chi^2$s of 1.92 and 2.4 (for 111 d.o.f.) for the high and low states, respectively. The residuals to this fit indicate a clear soft excess at low energies. The shape of the excess, which begins to dominate the spectrum at ~2 keV, is illustrated in Figure 2. To produce this figure, the high and low state A0 data were averaged together and fitted above 2 keV with a uniformly absorbed power law (having $\Gamma_{2-10} \sim 1.4$). The low-energy data were then added back in.

#### 3.2.1. *Single-Component Fits to the Primary Excess*

*Partial covering.*—In a first attempt to interpret the soft excess, a model consisting of a power law covered by a spatially nonuniform cold absorber ("partial covering") including a narrow Gaussian for the Fe K line was fitted to the entire 0.4–11.0 keV bandpass. This model provides a good statistical fit to both observations (Table 2A) with $\chi^2_\nu = 0.96$ and 1.12, respectively. However, the best-fit covering fraction *decreases* by a significant amount as the source dims. This is illustrated in Figure 3, which shows a plot of the confidence contours for covering fraction versus column density. Figure 4 shows a comparison of the A0 data and best-fit partially covered continuum model (folded through the BBXRT response) for the high and low states. From this figure it can be seen that since the 0.4–1.5 keV count rate remains constant while the hard flux decreases, the derived covering fraction must decrease as the continuum source becomes fainter. This implies that either the absorber "knew" about the source flux variability or changed by coincidence in such a way as to mimic a constant flux at low energies. The unfolded spectrum corresponding to Figure 4 is illustrated in Figure 5, which is a perfectly adequate representation of the X-ray spectral shape observed by BBXRT.

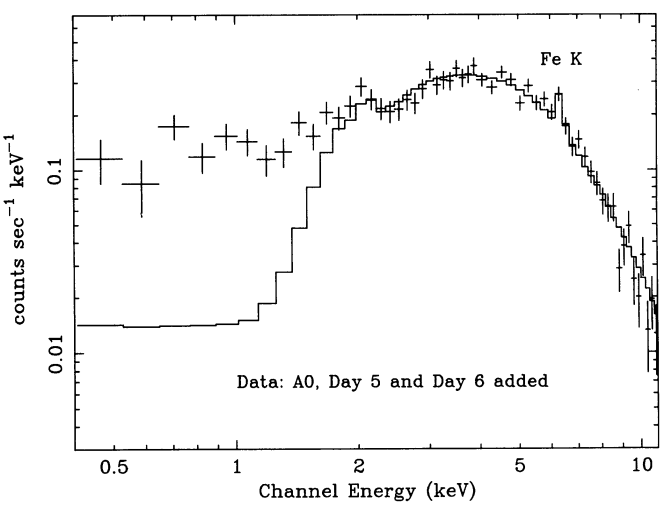


FIG. 2.—Illustration of the soft X-ray excess observed with BBXRT. To produce this plot, the data were fitted above 2 keV with a uniformly absorbed power law, and the lower energy points were added back in. The *solid line* represents the model.

TABLE 2

SINGLE COMPONENT FITS TO THE NGC 4151 SOFT EXCESS

A. MODIFIED ABSORPTION FITS

| PARAMETER | PARTIAL COVERING High | PARTIAL COVERING Low |
|---|---|---|
| $\Gamma$ | $1.50^{+0.15}_{-0.11}$ | $1.32^{+0.13}_{-0.13}$ |
| $N_H$ | $4.91 \pm 0.40$ | $5.24 \pm 0.63$ |
| $f_c$ | $0.973^{+0.007}_{-0.005}$ | $0.943^{+0.011}_{-0.016}$ |
| $F_{low}$ | $0.19 \pm 0.02$ | $0.19 \pm 0.02$ |
| $F_{med}$ | $19.1 \pm 0.3$ | $12.0 \pm 0.3$ |
| $\chi^2/\nu$ | 105/109 | 122/109 |

| PARAMETER | WARM ABSORBER High | WARM ABSORBER Low |
|---|---|---|
| $\Gamma_{input}$ | 1.5 | 1.5 |
| $N_H$ | $8.71^{+0.63}_{-0.58}$ | $9.13^{+0.65}_{-0.61}$ |
| log $U$ | $0.42^{+0.06}_{-0.10}$ | $0.55^{+0.11}_{-0.09}$ |
| $F_{low}$ | $\sim 0.20$ | $\sim 0.19$ |
| $F_{med}$ | $19.0 \pm 0.8$ | $11.6 \pm 0.6$ |
| $\chi^2/\nu$ | 110/110 | 127/110 |

B. SEPARATE SPECTRAL COMPONENT FITS

| PARAMETER | BREMMSTRAHLUNG High | BREMMSTRAHLUNG Low |
|---|---|---|
| $\Gamma$ | $1.39^{+0.16}_{-0.07}$ | $1.25^{+0.15}_{-0.10}$ |
| $N_H$ | $4.27^{+0.50}_{-0.27}$ | $4.55^{+0.33}_{-0.40}$ |
| $kT$ | $1.00^{+0.72}_{-0.44}$ | $1.79^{+4.1}_{-0.63}$ |
| $F_{low}$ | $\sim 0.22$ | $\sim 0.21$ |
| $F_{med}$ | $19.1 \pm 0.5$ | $12.0 \pm 0.5$ |
| $\chi^2/\nu$ | 104/108 | 124/108 |

| PARAMETER | POWER LAW High | POWER LAW Low |
|---|---|---|
| $\Gamma$ | $1.50^{+0.15}_{-0.11}$ | $1.40^{+0.10}_{-0.18}$ |
| $N_H$ | $4.95^{+0.23}_{-0.45}$ | $5.64^{+0.50}_{-0.42}$ |
| $A(1)/A(2)$ | 0.03 | 0.06 |
| $F_{low}$ | $0.20 \pm 0.03$ | $0.20 \pm 0.02$ |
| $F_{med}$ | $18.9 \pm 0.5$ | $11.8 \pm 0.4$ |
| $\chi^2/\nu$ | 105/109 | 123/109 |

NOTES.—The column density $N_H$ is given in units of $10^{22}$ cm$^{-2}$. $F_{low}$ is the 0.5–1.5 keV flux and $F_{med}$ is the 2–10 keV flux given in units of $10^{-11}$ ergs cm$^{-2}$ s$^{-1}$. All fits include a narrow Fe K line with energy fixed at 6.38 keV. Except for fluxes, errors are 90% confidence for two interesting parameters. All soft excess components are absorbed by an additional column of $N_{Hgal} = 0.02 \times 10^{22}$ cm$^{-2}$. $A(1)/A(2)$ is the ratio of 1 keV normalizations of the soft excess power law (the reflected component in the scattering model) and the direct power-law continuum.

The data also suggest that the shape of the 2–11 keV continuum has changed between the high and low states, although we cannot distinguish between an increase in the column density or a spectral flattening with decreasing flux. The two-dimensional confidence contours for photon index versus $N_H$ obtained from the 0.4–11 keV partial covering fits are shown in Figure 6. The 90% contours do not overlap, indicating that either the index or the column density has varied between the high and low states. A ratio of the high to the low state data

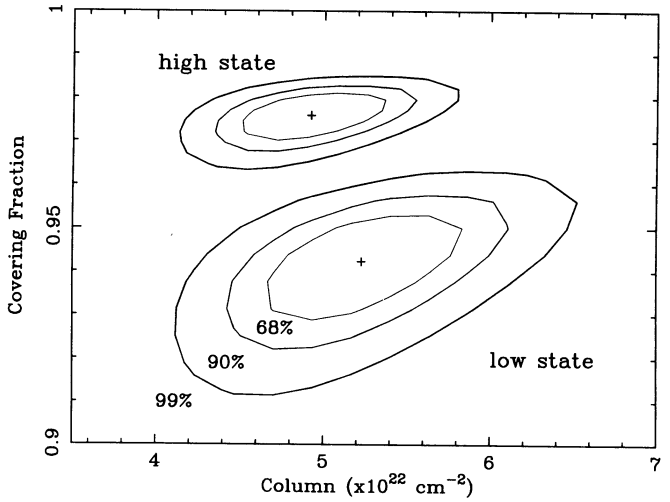


FIG. 3.—Two-dimensional confidence contours for the covering fraction vs. the observed column density for partial covering fits to the 0.4–11.0 keV data. The crosses mark positions of minimum $\chi^2$. Contours are 68%, 90%, and 99% confidence.

(Fig. 7) provides a model-independent test of this change. The ratio remains flat ($\sim 1$) between 0.4–1.2 keV, and remains flat from 5 to 10 keV. Such a shape can be produced either by an increase in the column density in the low state, or by a flattening of the photon index in the low state. A slight increase in column density or flattening of the spectrum does not alter our original result that the covering fraction is observed to decrease as the continuum source dims.

There is evidence for a positive correlation between spectral index and source flux in NGC 4151 (Yaqoob & Warwick 1991), and so we may expect to observe a slight flattening of the spectrum when the 2–10 keV flux decreases by 40%. On the other hand, it is also possible that the column density can change on short timescales. A change in column density can be interpreted in one of two ways. If the X-ray absorber is clumpy and located close to the continuum source, then variability of the column density is predicted to occur as clouds pass in front

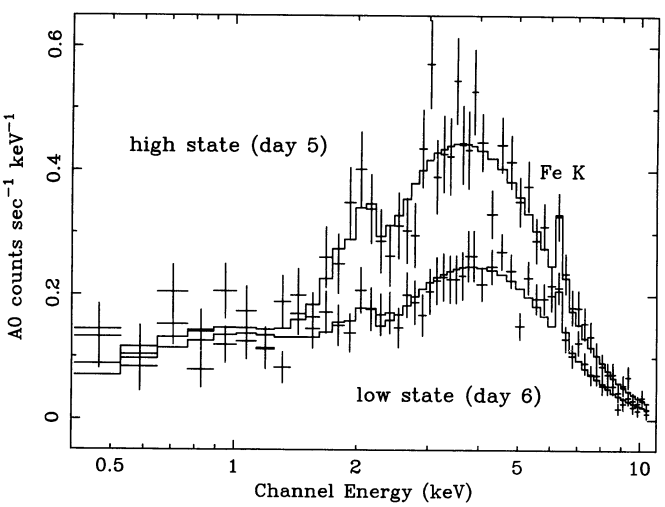


FIG. 4.—The A0 data and best fit partial covering model (*solid line*) for the high and low states. The Fe K$\alpha$ emission line is included in the fits. The edge at 2.2 keV is due to absorption by the mirrors.

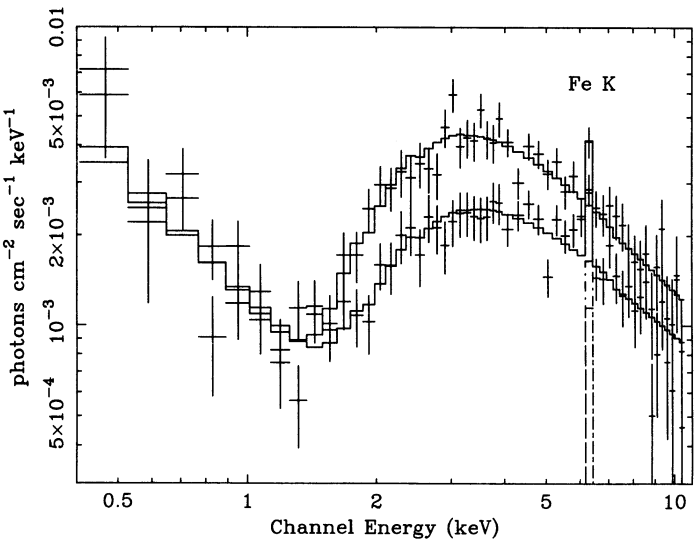


FIG. 5.—Unfolded spectrum corresponding to the partial covering fit that is illustrated in Fig. 4. The *solid line* represents the best-fit partial covering model.

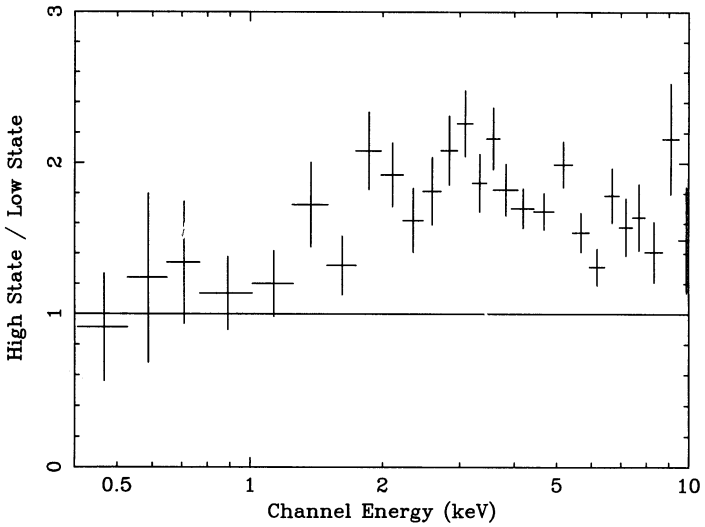


FIG. 7.—Ratio of the high to low state data in pixel A0

of the X-ray source. The crossing timescale of a single cloud depends on the ratio of the cloud size to the central source size as well as the transverse velocity of the cloud. For a cloud moving at $10^4$ km s$^{-1}$ having a size of $10^{14}$ cm (which is assumed to be the same as that of the X-ray source) Reichert, Mushotzky, & Holt (1986) calculate a cloud transit time of 2 days, which would be consistent with a 1 day change in the column. However, an increase in the column as the flux dims might imply that the soft excess is due to a change in the ionization state of the absorber on short timescales (see below for a test of this model).

Besides the fact that the low-energy flux does not track the high-energy flux as the source dims, there is another problem with a partial covering description of the NGC 4151 spectrum. We find that the partial covering model does not provide a consistent description of the broad-band spectrum during the low state. Figure 8 shows the confidence contours for the column density versus the photon index, obtained from fitting

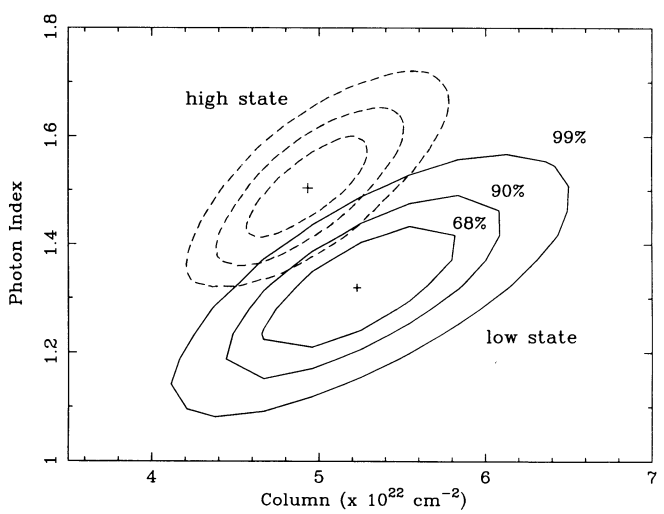


FIG. 6.—Two-dimensional confidence contours of photon index vs. column density for partial covering fits to the 0.4–11.0 keV data. The *crosses* mark positions of minimum $\chi^2$. Contours are 68%, 90%, and 99% confidence.

a partial covering model to two different bandpasses: 0.4–11 keV and 2–11 keV. During the high state, the contours overlap (Fig. 8*a*). However, during the low state, they do not (Fig. 8*b*) indicating that the result obtained depends on the assumed bandpass. Also, the derived covering fraction for the low state when fitting the 2–10 keV continuum alone is ~0.89, lower than that obtained from fitting the 0.4–11.0 keV continuum (~0.94). The reason for this apparent difference in derived covering fraction with bandpass is that there are additional residuals located at ~2 keV in the low state (discussed in § 3.2.3 and shown in Fig. 13*b* below) that are driving the 2–11 keV fit. One thing Figure 8 does suggest is that care should be taken in interpreting partial covering results for NGC 4151 from low flux-state proportional counter data when the low-energy instrumental cutoff is 1–2 keV.

*Ionized absorber.*—The primary soft excess in NGC 4151 has been modeled in terms of an ionized (or "warm") absorber (Yaqoob et al. 1989; Yaqoob & Warwick 1991). However, the models previously applied only treated absorption along the line of sight without including other physical processes. We have therefore attempted to model the soft excess with an improved ionized absorber model (Netzer 1993), which includes all emission processes in the gas as well as Compton reflection from the ionized material. Netzer (1993) finds that contributions from low-energy emission features can both dilute absorption edges and complicate the variability pattern of the low-energy flux. The most important absorbing element in the gas is oxygen, and the strongest absorption edges are due to O VII at 739 eV and O VIII at 870 eV, while emission from oxygen and iron dominates.

The model consists of a "normal" AGN input spectrum as described in Netzer (1993) with $\alpha_{ox} = 1.2$, extending out to 40 keV. The continuum is fully covered by a single large cloud and the covering fraction for the entire cloud system is 0.5. The free parameters in the model are the normalization of the power law, the ionization parameter, and the column density of the absorber. The dimensionless ionization parameter is defined as $U = F_{ph}/N_H c$ where $F_{ph}$ is the incident ionizing photon flux, $N_H$ is the hydrogen number density, and $c$ is the speed of light. For solar composition, the abundance ratios are given by (He, C, N, O, Ne, Mg, Si, S, Fe):H = (1000, 3.7, 1.1, 8.0, 1.0, 0.35, 0.33, 0.16, 4.0) × $10^{-4}$. The continuum shape

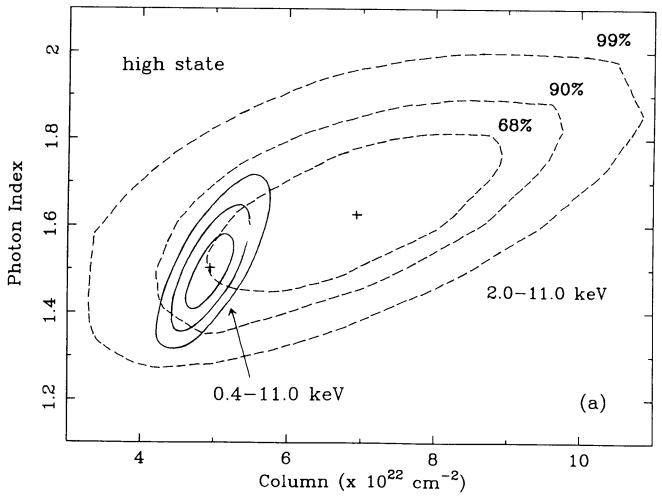


FIG. 8*a*

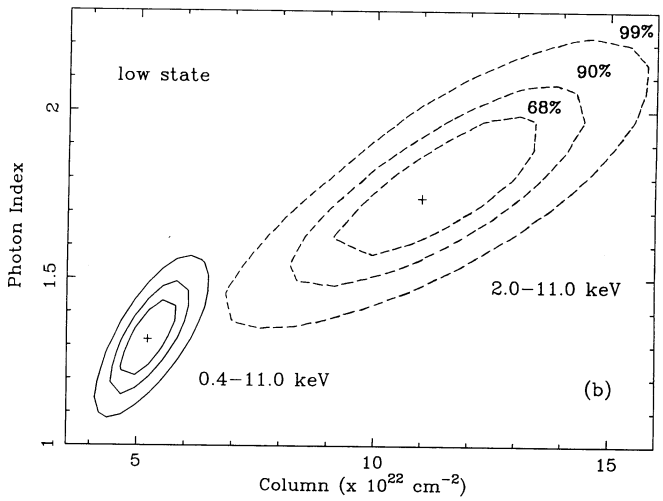


FIG. 8*b*

FIG. 8.—Confidence contours for $\Gamma$ vs. $N_H$ for (*a*) the high state, and (*b*) the low state. The contours for the 2–10 keV partial covering fits (*dashed lines*) are compared to those from the 0.4–11 keV partial covering fits (*solid lines*). The *crosses* mark positions of minimum $\chi^2$. Contours are 68%, 90%, and 99% confidence.

cannot be varied during the fitting procedure, and so different models have been generated for different values of the input spectral index. For NGC 4151, a value of $\Gamma = 1.5$ was chosen as the X-ray slope to most closely match the observed 4–11 keV indices. Models were calculated having various elemental abundances.

Initially, we examined a model having solar metal abundance; this model is illustrated in the lower half of Figure 9. However, a solar abundance model did not provide a good description of the data since we do not observe the strong, predicted oxygen edges. The top curve in Figure 9 shows a similar model having oxygen at $\frac{1}{2}$ solar abundance with all other metals at solar abundance. This model provides the most adequate description of the data giving a $\chi^2_\nu$ of 1.0 and 1.15 for the high and low states, resepctively (Table 2A).

Although the model predicts many emission features at low energies, we do not observe any discrete line complexes below 1.4 keV. To illustrate the featurelessness of the low energy continuum, Figure 10 shows the ratio of the 0.4–1.4 keV A0 data (high and low states) to a simple power-law model. This model was chosen to obtain a flat continuum against which to search for lines. The data are binned roughly to the BBXRT resolution (each bin is $\sim 100$ eV wide). There are no obvious features, and 90% confidence upper limits placed on any line emission between 0.4–1.4 keV are less than 70 eV in equivalent width (EW), with the exception of 0.7 keV where a 200 eV EW line is allowed. The features predicted by the ionized absorber model are rather weak, however, (spanning a range of 10–100 eV EW with $\sim 50$ eV EW being typical), and so we are not particularly sensitive to them.

One problem with an ionized-absorber description of the primary soft excess is that we do not observe the soft flux track the hard flux. A strong prediction of the ionized absorber model is a temporal one, and that is that the softness ratio $R_S = F_{X(0.5-1.5\,\mathrm{keV})}/F_{X(2-10\,\mathrm{keV})}$ should remain the same or even decrease slightly as the 2–10 keV flux decreases. This is because

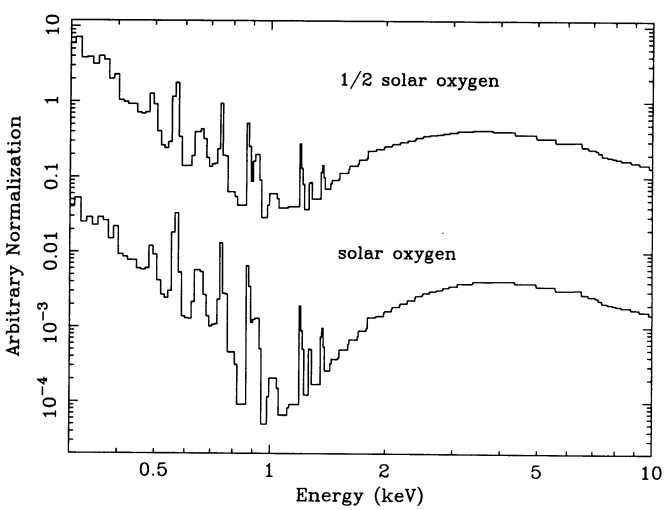


FIG. 9.—Ionized absorber models that are discussed in § 3.2.1 of the text

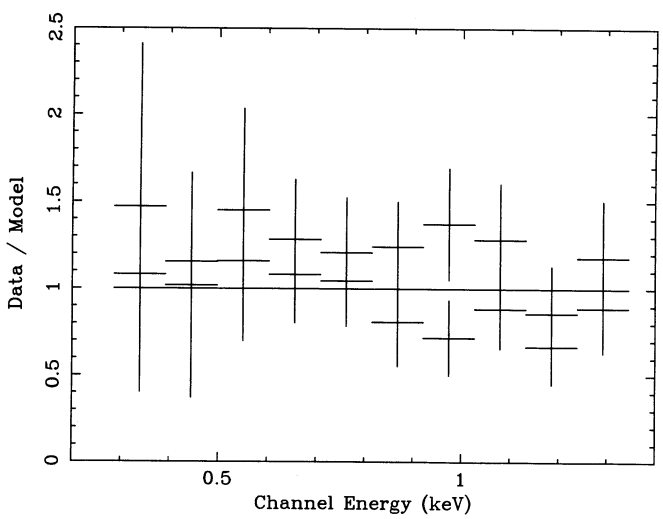


FIG. 10.—Ratio of the 0.4–1.4 keV data to a best-fit power-law continuum ($\Gamma = 1.7$) absorbed by Galactic $N_H$. This model was used to obtain a flat continuum against which to search for features.

the recombination timescale for gas along the line of sight is short ($\sim 100$ s). For an ionized-absorber description of the high state (Table 2A) $R_S \sim 0.01$, and is predicted to be within 0.01–0.005 in the low state. However, the softness ratio is observed to increase from $\sim 0.01$ during the high state to 0.017 during the low state which is the opposite of what is predicted. This has the effect of causing the measured ionization parameter to *increase* when the source dims. This is illustrated in Figure 11 which shows the two-dimensional contours for $U$ versus $N_H$. The 90% confidence contours do not overlap, and the change in ionization parameter goes in the "wrong" direction (see discussion in § 4.1.2).

Another problem for the ionized absorber model is that the derived ionization parameter is inconsistent with the ionization parameter that is implied for the absorbing material based on the observed energy of the Fe K edge. The Fe K edge energy is found to be $7.46 \pm 0.23$ keV (Paper I), corresponding to Fe V-XVII (Makishima 1986). However, an ionization parameter of $\log U \sim 0.5$ implies that iron should be ionized to Fe XIX (Makishima 1986) giving an edge energy of 7.9 keV (Yaqoob & Warwick 1991). A similar problem for a warm absorber description of the soft excess was found by Yaqoob & Warwick (1991) from an analysis of *Ginga* data. They determined that the energy of the iron K edge in NGC 4151 rules out the high value of the ionization parameter as measured from their warm absorber spectral fits. We follow the interpretation of Yaqoob & Warwick (1991) that the Fe K edge energy does not support a warm absorber origin for the entire soft excess in NGC 4151. However, the Fe K edge energy is consistent with a multiple component description of the soft excess in which less than 50% of the flux in the soft excess arises from an ionized absorber with a lower ionization parameter (discussed in § 4.3).

*Thermal Emission.*—For a thermal bremsstrahlung fit to the primary soft excess the temperature is not well constrained (Table 2B). However, our values of $kT = 1.0$–$1.7$ keV are in rough agreement with $kT = 0.58\ (+2.8, -0.1)$ keV seen in the *EXOSAT* data (Pounds et al. 1986). Setting the thermal component to have $kT = 0.58$, we find the observed 0.2–1.0 keV flux to be $2.8 \pm 0.6 \times 10^{-12}$ ergs cm$^{-2}$ s$^{-1}$ which is very close to the value measured by Pounds et al. (1986) of $4.0 \times 10^{-12}$ ergs cm$^{-2}$ s$^{-1}$. The intrinsic luminosity of this component (corrected for Galactic absorption) for $kT = 0.58$ is $\sim 2 \times 10^{41}$ ergs s$^{-1}$, which is similar to their value of $2.6 \times 10^{41}$ ergs s$^{-1}$. Therefore, we conclude that for a thermal description of the soft excess, our results are consistent with those observed by Pounds et al. (1986). For our best fit of $kT = 1.0$ keV, the 0.3–4 keV flux in the soft component is $(3 \pm 0.5) \times 10^{-12}$ ergs cm$^{-2}$ s$^{-1}$. This gives a luminosity of $(1.55 \pm 0.25) \times 10^{41}$ ergs s$^{-1}$. Both the BBXRT and *EXOSAT* luminosities are higher than the 0.1–3 keV luminosity observed in the extended component of $\sim 3.0 \times 10^{40}$–$1.2 \times 10^{41}$ ergs s$^{-1}$ (Elvis et al. 1983, 1990).

The problem with a thermal model is that at temperatures of $kT = 0.58$–$1.7$ a simple free-free continuum has no physical meaning since we would expect to see line emission associated with a hot plasma (unless, of course, there are no metals). The BBXRT data reject a Raymond-Smith plasma model for the best-fit thermal temperatures, as no evidence of strong low-energy line emission is seen (Fig. 10). The 90% confidence upper limits to the metal abundance are 0.10 solar and 0.24 solar for the high and low states, respectively, using the best-fit thermal temperatures given in Table 2B.

*Scattering.*—Since the partial covering model provides a good analytical description of the data in the high state, this naturally leads to the possibility that the soft excess may be due to scattering of the central continuum instead of leakage. In this scenario, a finite column density cloud, large enough to absorb all energies between the Lyman limit and $\sim 1$ keV, is obscuring the direct line of sight. At this stage we only test the idea that such obscuring gas is neutral.

A fourth model was constructed consisting of two power laws having the same spectral index, one absorbed by a high intrinsic column and the other by Galactic $N_H$ (Table 2B). This model, illustrated in Figure 12, is algebraically the same as a partially covered continuum. However, we have defined it as a new model in order to stress the fact that this provides a different physical description of the data. The fraction of the continuum scattered can be measured in two ways. First, the ratio of the fluxes of the soft X-ray power law and the 2–11 keV power law at 1 keV [$A(1)/A(2)$ in Table 2B] provides a ratio of the

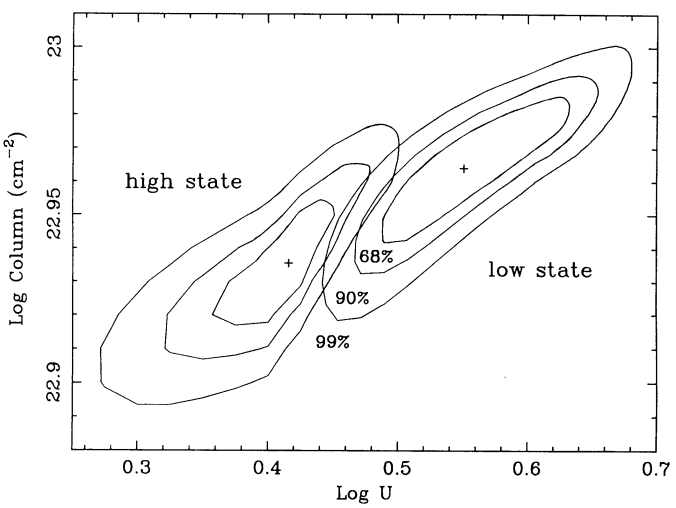


FIG. 11.—Confidence contours for the ionization parameter vs. the observed column density for a $\frac{1}{2}$ solar oxygen ionized-absorber description of the soft excess. The *crosses* mark positions of minimum $\chi^2$. Contours are 68%, 90%, and 99% confidence.

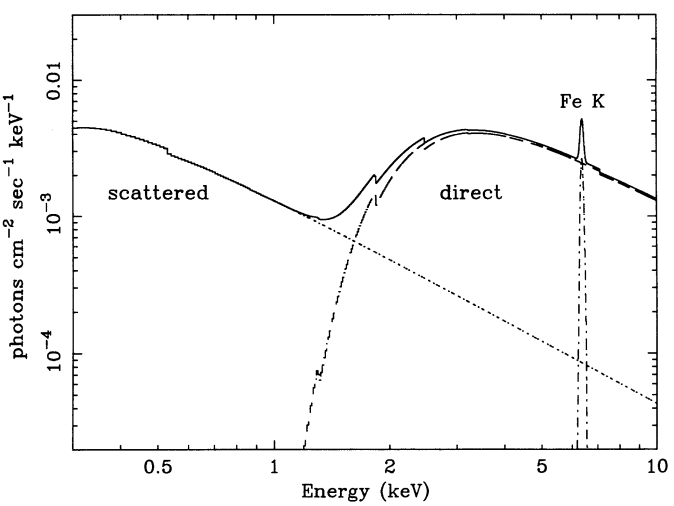


FIG. 12.—Scattered continuum model used the soft excess

scattered to direct continuum. The fraction scattered can also be determined by extrapolating the unabsorbed high-energy slope to lower energies and measuring the strength of the observed low-energy continuum relative to the extrapolation. Both methods give a fraction scattered of $\sim 3\%$–$4\%$ for the high state and 5%–6% for the low state. An increase in the fraction scattered is consistent with the temporal predictions of the model, since we expect the ratio to increase when the source flux decreases if the nuclear continuum is scattered into our line of sight. This is due to a delay in the response of the scattered component to the continuum. The measured column density absorbing the scattered component is consistent with the Galactic column density and the 90% confidence upper limit is $1.2 \times 10^{21}$ cm$^{-2}$.

The intrinsic column density (that of the obscuring cloud) measured from the scattering model is $\sim 5 \times 10^{22}$ cm$^{-2}$ (Table 2*B*). This column is much higher than the UV absorbing column found by Kriss et al. (1992) of $6 \times 10^{17}$–$6 \times 10^{20}$ cm$^{-2}$, and implies that a single large obscuring cloud is not responsible for both the UV and X-ray absorption. One possible explanation (Weaver 1994), in the content of NGC 4151 being somewhat like a Seyfert 2 (§ 4.2.2), is that the X-ray absorber is the same as the gas responsible for the optical broad lines (the broad line region) while the UV absorber is a low column density torus responsible for collimating the UV radiation (Kriss et al. 1993).

### 3.2.2. *SSS + MPC Observations*

To further investigate the variability pattern of the soft excess in NGC 4151, we examined simultaneous *Einstein Observatory* Solid State Spectrometer (SSS) and Monitor Proportional Counter (MPC) data covering days 146–148 of 1979. During these observations, the 2–10 keV continuum flux level is similar to the low flux state in BBXRT. Table 3 gives the observed count rates in various energy bands. An interesting variability pattern is seen. The 0.6–1.5 keV count rate and the 4–10 keV count rate change by $\lesssim 10\%$ (although the errors cannot rule out maintaining a constant flux level) while the 1.5–4 keV count rate changes by $\sim 20\%$. The best-fit MPC photon index is $1.4 \pm 0.3$. If we assume it remains constant during the three observations, the only way to reconcile the SSS and MPC data is if the column density decreases by $\sim 40\%$ (from $\sim 13.5 \pm 3.0 \times 10^{22}$ to $8.5 \pm 1.0 \times 10^{22}$ cm$^{-2}$) in 1 day. A partial covering fit to the SSS and MPC data allows the covering fraction to remain constant, and so we cannot rule out partial covering as being the best descriptor of the data. For the best-fit absorption values (with $\Gamma = 1.4$), the 0.5–1.5 keV flux is $(4 \pm 1.0) \times 10^{12}$ ergs cm$^{-2}$ s$^{-1}$ which is consistent to within a factor of 2 with the flux obtained for a partial covering fit to the BBXRT data (see Table 2A).

### 3.2.3. *Silicon Features*

Differences between the high- and low-state spectra due to possible features can be seen in the residuals to the low-state data for a partial covering description, a thermal description, and a scattering description of the soft excess. In a plot of the ratio of the 0.4–11.0 keV data to the partial covering model for the high state (Fig. 13*a*) there are no systematic residuals observed greater than 10%. However, in the low-state ratio (Fig. 13*b*) a broad hump is visible between 4–8 keV (a possible explanation of this "hump" as a broad emission line is given in Paper I) while there is a positive "feature" between 1.5 and 3.0 keV. This indicates that the partial covering model, while statistically a good fit, does not provide a good analytical description of the entire continuum in the low state. The 1.5–3.0 flux component may not vary and is apparently swamped when the source is in a high state. The fact that this portion of the total soft X-ray excess seen by BBXRT above 1.5 keV does *not* track the 2–10 keV continuum flux is contrary to behavior which has previously been reported in NGC 4151 (Yaqoob & Warwick 1991).

The 1.5–3.0 keV residuals can be well described with two narrow Gaussians, which provide a reasonable physical interpretation. Setting the line energies to be 1.865 and 2.01 keV for He-like and H-like Si recombination (Si XIII and Si XIV), $\Delta\chi^2 = 7$ which is significant at 90% confidence for the addition of 2 d.o.f. using the F-test. The equivalent widths of the lines, measured with respect to the absorbed continuum, are $110 \pm 90$ eV and $60 \pm 50$ eV (90% confidence errors) and the flux in each line is $\sim 0.001$ and $\sim 0.0005$ photons cm$^{-2}$ s$^{-1}$, respectively. The H-like/He-like line ratio, although not well constrained by the data, is $0.55^{+4.95}_{-0.5}$. For silicon recombination in a plasma this indicates a temperature of greater than $10^{6.8}$ K (Raymond & Smith 1977). The total flux in the lines is found to be $\sim 7 \times 10^{-13}$ ergs cm$^{-2}$ s$^{-1}$ which gives a luminosity of $3.4 \times 10^{40}$ ergs s$^{-1}$ at 20 Mpc. The line flux corresponds to $\sim 8\%$ of the total 0.1–3 keV flux which is about half that seen in the HRI extended component (Elvis et al. 1983).

The presence of Si Ly$\alpha$ at 2.01 keV restricts the temperature of the region where the Si originates to be at least $10^{6.8}$ K, if it is a collisionally excited gas. At this and higher temperatures for a plasma, we should see even stronger emission features due to Fe L and S (2.460 keV). The lack of these spectral signatures indicates that the line-emitting plasma, if collisionally excited, is most likely in a nonequilibrium state, as is often seen in the spectra of supernova remnants (e.g., Hamilton, Sarazin, & Szymkowiak 1986). For a hot, photoionized gas, the temperature is lower and may be consistent with the temperature of the proposed scattering medium (discussed in § 4.2.2). A full model of such gas is beyond the scope of the present paper.

## 4. DISCUSSION

We find that the primary soft excess in NGC 4151 (that between 0.4 and 1.5 keV) comprises essentially a featureless continuum that does not vary on short timescales and is consistent in shape and flux to the nonvariable soft excess observed with *EXOSAT* (Pounds et al. 1986). However, in

TABLE 3

SSS + MPC OBSERVATIONS OF NGC 4151

| Day (1979) | 0.6–1.5 keV Count Rate (SSS counts s$^{-1}$) | 1.5–4.0 keV Count Rate (SSS counts s$^{-1}$) | 4–10.0 keV Count Rate (MPC counts s$^{-1}$) |
|---|---|---|---|
| 146..... | $0.13 \pm 0.01$ | $0.22 \pm 0.01$ | $5.6 \pm 0.6$ |
| 147..... | $0.15 \pm 0.01$ | $0.28 \pm 0.01$ | $6.2 \pm 0.6$ |
| 148..... | $0.14 \pm 0.01$ | $0.28 \pm 0.01$ | $6.0 \pm 0.6$ |

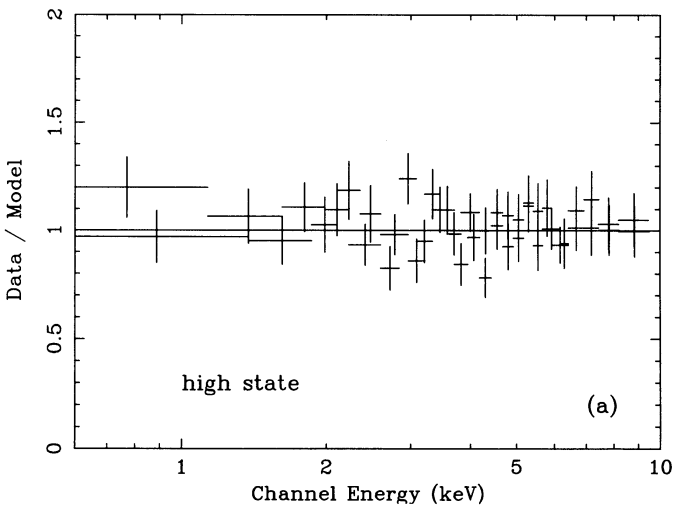


FIG. 13*a*

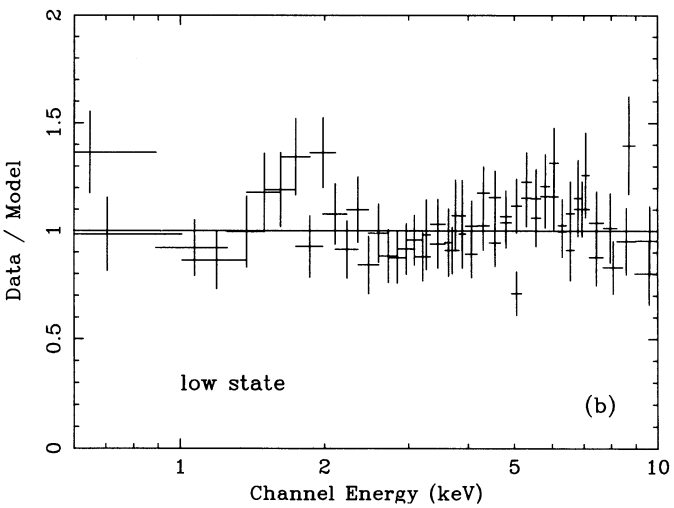


FIG. 13*b*

FIG. 13.—Ratio of the broad-band data to the best-fit partial covering model (described in § 3.2.1): (*a*) high state; (*b*) low state. Additional binning has been applied to the data.

contrast to *EXOSAT* results, for a single component description of the soft excess the BBXRT data actually imply that the partial covering excess found by Holt et al. (1980) is the same as the nonvariable excess observed by Pounds et al. (1986) and Perola et al. (1986). Although BBXRT has provided the best indication of the form of the excess to date, better signal-to-noise ratio data is needed to determine the difference between models with very similar spectral shapes and to detect weak features associated with an ionized absorber. In §§ 4.1 and 4.2, we determine which single-component characterizations of the primary excess may have physical implications.

### 4.1. *Modified Absorbing Column*

#### 4.1.1. *Partial Covering*

A partial covering description of NGC 4151 has historical significance as it was the first model used to describe the soft excess. Holt et al. (1980) preferred it based on simplicity arguments. The partial covering model still provides an excellent analytical description of the primary excess. However, if we attempt to interpret this model physically, there are problems. For clouds passing across the line of sight we expect the low-energy X-ray flux to track the 2–10 keV continuum flux. There is no reason *a priori* to expect the covering fraction to "know about" the flux change and adjust at the same time in just such a way as to cause the soft flux to remain constant; however, this is what our observations imply. Therefore, we conclude that a partial covering description of the soft excess is unlikely.

#### 4.1.2. *Ionized Absorber*

Ionized or "warm" absorber models are becoming increasingly popular to explain the soft excesses seen in the spectra of quasars (Halpern 1984; Pan, Stewart, & Pounds 1990; Fiore et al. 1993) and Seyfert galaxies (Yaqoob et al. 1989; Nandra et al. 1991; Turner et al. 1992). In the simplest "absorption-only" model, as the ionizing continuum increases (providing more hard photons at the face of the cloud) the ionization parameter increases since the line-of-sight absorbing clouds respond to changes in the ionizing flux on timescales of minutes. Therefore, we expect the ionization parameter to be proportional to $F_{X(2-10)}$ and the softness ratio to remain roughly constant. For NGC 4151 we observe the ionization parameter to be inversely proportional to $F_{X(2-10)}$ and the softness ratio is seen to increase. Also, the Fe K edge energy is inconsistent with having been produced in gas with the same ionization parameter as the low-energy absorber. This allows us to rule out a line-of-sight ionized absorber as the sole source of the soft X-ray excess in NGC 4151.

Possibly a more physical scenario is that there is a significant contribution to the soft excess in the form of line emission from clouds out of the line of sight which, because of the time lag, would not change on the same timescale as the continuum. The question then becomes: how much of the soft excess can be due to the reduced opacity of the absorber along the line of sight? We examined the data and assumed first that all of the soft excess observed in the high state is due to a warm absorber, and second, that the ionization parameter decreases during the low state to $\sim\frac{1}{2}$ that of the high state, consistent with the change in the 2–10 keV flux. With these assumptions, an ionized absorber can make up only 40% of the soft excess in the low state.

We conclude that this particular subset of ionized absorber models, although they give an adequate description of the soft excess, do not adequately predict the lack of temporal variations that are observed. Although we have not yet included time delay and reverberation effects in our analysis, we find that an ionized absorber cannot be responsible for the entire soft excess unless there is a significant contribution from photoionized clouds that lie out of the line of sight.

### 4.2. *Spatially Extended Component*

An alternative explanation of the BBXRT soft excess is that it is not directly related to the continuum but may be emission from a spatially extended component. A thermal continuum provides an excellent description of the primary soft excess, and our best-fit energy and flux in the soft component is consistent with that observed previously (Pounds et al. 1986). In addition, we find that the *Einstein* SSS and MPC data also show the majority of the soft excess to remain constant over a

two day time scale with a flux consistent to within a factor of 2 with that observed by BBXRT.

In addition, spatially extended soft X-rays have been discovered in NGC 4151 to account for at least 15% of the 0.1–3.0 keV flux (Elvis et al. 1983). Assuming a thermal spectrum absorbed by the Galactic column, Elvis et al. (1983, 1990) find the luminosity of this extended component to be between $3.0 \times 10^{40}$ and $1.2 \times 10^{41}$ ergs s$^{-1}$. This could make up $\sim\frac{1}{2}$ of the luminosity observed by BBXRT for a thermal description of the data ($kT = 0.58$). However, the HRI observation is only sensitive to extended emission on a larger than kiloparsec scale, so there is almost certainly "extended" emission unresolved by the HRI.

#### 4.2.1. *Hot Gas in Collisional Equilibrium*

Much discussion in the literature has focused on the soft excess/extent as being emission from the hot intercloud medium (HIM) proposed to constrain the narrow-line clouds. For a hot, photoionized gas to pressure confine the narrow-line clouds, it is likely to be at its Compton temperature (Krolik, McKee, & Tartar 1981; Krolik & Vrtilek 1984). For the continuum chosen to represent NGC 4151, this is $\sim 2.7 \times 10^7$ K. For a collisionally excited plasma there is no such temperature limit, and higher temperatures can occur, provided the density is high enough (i.e., the ionization parameter is low enough). In such gas, for temperatures between $1 \times 10^6$ and $2 \times 10^7$ K, the cooling is dominated by line emission and we expect to observe a blend of lines centered between 0.8 and 1.2 keV due mostly to Fe L. For higher temperatures ($>2$–$3 \times 10^7$ K) the emissivity is dominated by the free-free continuum.

The upper limit to the Fe abundance from a Raymond-Smith plasma fit to the BBXRT soft excess is 0.03 solar at a temperature of $1 \times 10^7$ K. Setting the abundance in the gas to 0.5 solar, we find that the plasma temperature must be at least $T = 3.5 \times 10^7$ K and setting the abundance to solar the temperature must be at least $5.2 \times 10^7$ K, both of which are higher than the temperature expected for a photoionized confining medium. As explained, a collisionally ionized gas must have a higher density, and therefore a higher pressure, to keep such high temperatures without being fully ionized by the central radiation source. Thus, it cannot be in pressure equilibrium with the NLR gas. We therefore conclude that the excess cannot be due to an equilibrium plasma with a temperature of $10^6$–$10^7$ K, and it is not likely to be emission associated with the NLR confining medium.

#### 4.2.2. *Electron Scattered Radiation*

Although we clearly see the continuum and the broad emission-line region in NGC 4151, much evidence has accumulated to support an edge-on geometry for the central region of the galaxy (Clavel et al. 1987; Maoz et al. 1991; Maisack & Yaqoob 1991; Kriss et al. 1993). In the context of the Unified Model, this geometry makes NGC 4151 similar to a Seyfert 2 galaxy. If we assume NGC 4151 is like a Seyfert 2 (i.e., having an optically thick torus that collimates the UV radiation), we might expect to observe some fraction of the X-ray continuum that has been reprocessed and scattered into our line of sight by the electron scattering zone (as in NGC 1068; Antonucci & Miller 1985; Marshall et al. 1993). A scattered continuum also provides a good description of the soft X-ray data and is consistent with the lack of short-term variability.

The observed fraction scattered provides a measure of the optical depth of the scattering zone. From the day 5 observation we obtain a fraction of 0.03. The Compton depth is given by $\tau_{es} \sim f_{scatt}(c_f \times \Omega/4\pi)^{-1}$ where $\Omega/4\pi$ is the solid angle, and $c_f$ is the covering fraction. Kriss et al. (1993) find the ionization cone opening angle in NGC 4151 to be $\sim 70°$ which gives a solid angle of $\sim 0.2$ for the scattering zone. If we assume that the covering fraction is 1, then $\tau_{es} = 0.15$ in the scatterer.

Although the scattering zone acts essentially as a mirror at optical wavelengths, it will produce observable features at X-ray wavelengths. Based on the widths of the Balmer lines, Miller, Goodrich, & Mathews (1991) obtain an upper limit to the temperature of the scattering zone in NGC 1068 to be a few times $10^5$ K. If we assume the temperature of the scattering zone to be the same in NGC 4151, and if the reflector is not highly ionized, we should see oxygen absorption. For neutral material the oxygen optical depth is given by $\tau_{ox} = A_0(\sigma_{ox}/\sigma_{es})\tau_{es}$, where $A_0$ is the abundance of oxygen relative to solar and $\sigma_{es}$ are the absorption cross sections. This gives an expected optical depth of 9 with the assumed $\tau_{es}$ of 0.15.

The upper limit we measure for the oxygen edge at 532 eV is $\tau_{ox} = 1.0$, so we need to drastically reduce the oxygen abundance or have the scattering zone partially ionized. We then have the problem of suppressing emission from this zone, which requires a low electron density. Marshall et al. (1993) have found that it is possible to construct a model for the scattering region in NGC 1068, but only with reduced oxygen abundance. While there are other indications for abnormal oxygen composition in NGC 1068, this is not the case for NGC 4151, and the limit on the X-ray absorption is a severe limitation for a few times $10^5$ K scattering medium. The second component suggested by Marshall et al. (1993) is, in fact, more promising. This is a very hot, highly ionized gas, close to its Compton temperature. Such a gas can scatter the X-ray continuum very efficiently, without having a noticeable effect on the galaxy's broad optical emission-line properties (i.e., lines from such a gas will be broadened beyond recognition). There are no X-ray absorption features expected from this component and no other observational constraints except for a very weak polarized continuum at optical wavelengths.

### 4.3. *A Multiple Component Description of the Primary Excess*

We have found that no single-component description of the primary soft excess is ideal. Modified absorbing columns alone do not satisfy the temporal data while lack of strong spectral features causes problems for both thermal and scattered interpretations. This does not, however, mean that thermal or photoionized gas cannot contribute to the soft excess. If the major portion of the excess is due to scattering (§ 4.2.2), for example, then any emission features associated with a thermal component or an ionized absorber would be diluted. This would explain the fact that we do not observe strong features.

Although the quality of the BBXRT data does not allow us to constrain parameters for multicomponent fits to the soft excess, we can gain insight into the most likely possibility if some assumptions are made. First of all, the possible hint of an increase in derived column density seen between the high and low states (§ 3.2.1.1) suggests that a warm absorber may make some contribution to the soft excess. We have therefore examined a multi-component model that consists of an ionized absorber and a scattered component.

We performed this multicomponent test by fitting the high- and low-state data simultaneously with a power law ($\Gamma = 1.5$) and an ionized absorbing column, restricting $U$ for the low state to be equal to $\sim\frac{1}{2}U$ in the high state. A second power law was included (to represent scattering) with an index of 1.5 and

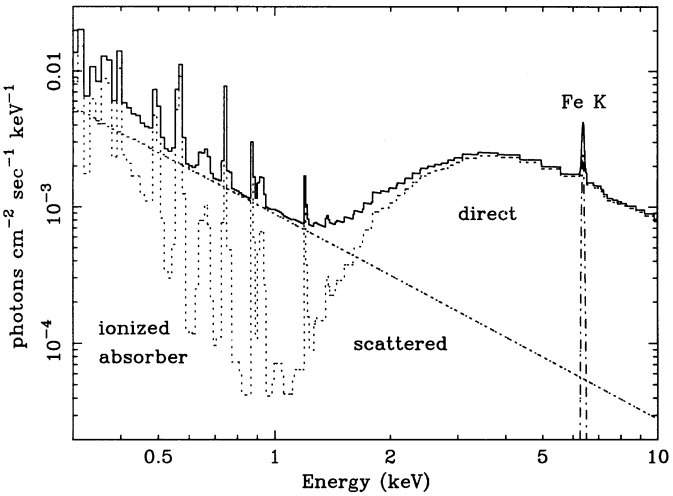


FIG. 14.—A multicomponent model for the soft excess that consists of a scattered continuum plus an ionized absorber. This model is discussed in § 4.3.

was restricted to have the same normalization for the high and low states. This model is illustrated in Figure 14. The fit, which allowed only six free parameters (one ionization parameter, two absorbing columns, one scattered power-law normalization and two direct power-law normalizations) gave $\chi^2/\nu = 219/220$, an improvement of 18 over the ionized absorber alone (significant at greater than 99% confidence). For this fit, log $U$ decreases to $\sim 0.01$ for the high state. An ionization parameter of log $U = 0.01$ predicts the energy of the Fe K edge to be $\sim 7.6$ keV (Yaqoob & Warwick 1991), which is consistent with the Fe K edge in the BBXRT data ($7.46 \pm 0.23$ keV). Although the multicomponent model does not improve the fit to the high state above the warm absorber alone ($\Delta\chi^2 = 1$ as compared to the fit in Table 2A), it drastically improves the fit to the low state giving $\chi^2/\nu = 110/110$ which is a $\Delta\chi^2$ of 17 (significant at $>99\%$) over the warm absorber result (Table 2A). When the low state data are modeled in this multicomponent way, the Si He$\alpha$ line at 1.86 keV is no longer significant. However, for a narrow Gaussian added at 2.01 keV, $\Delta\chi^2 = 3$ for 1 d.o.f. freedom implying Si Ly$\alpha$ is still marginally significant (at 90% confidence).

Even for this particular ionized absorber plus scattered continuum model, some fraction of the soft excess must vary. Upon close examination of the data, we find that the 0.5–1.5 keV flux is allowed to decrease by up to 20%, or $\frac{1}{2}$ the amplitude of the 2–10 keV flux, between the high and low states. From this we conclude that no more than 40%–50% of the soft excess can be due to a line-of-sight warm absorber and the other 50% must be due to a component which remains constant over a time period of at least one day and probably more (Pounds et al 1986; Perola et al. 1986). It can be seen in Figure 14 that the ionized absorber contribution to the excess will begin to dominate at the lowest energies (below 0.6 keV). Therefore, if an ionized absorber does contribute to the soft excess, the observed flux variability will be strongest at very low energies (provided that there is not cold gas in outlying regions that absorbs most of the $<0.5$ keV flux). Data with better signal to noise and (preferably) a lower bandpass coverage than BBXRT are needed to unambiguously detect this variability.

## 5. CONCLUSIONS

We have presented new X-ray spectral data on the well-studied Seyfert galaxy NGC 4151. To within the BBXRT sensitivity, the soft excess continuum is featureless and the softness ratio $R_S = F_{X(0.5-1.5)}/F_{X(2-10)}$ increases as the 2–10 keV flux decreases. These restrictions cause severe problems for any single-component description of the soft excess, and it is likely that the primary soft excess in NGC 4151 results from a combination of two components that are difficult to distinguish spectrally. Our major conclusions are summarized as follows:

1. We find that the soft X-ray excess in NGC 4151 between 0.4 and 1.5 keV comprises a continuum with no strong features either in emission (EW $< 100$ eV) or absorption.
2. We find that the 0.5–1.5 keV flux remains essentially constant over 17 hr, and is consistent with having varied by less than a factor of 2 over a 12 yr period.
3. The best-single component description of the excess is scattering of the hard X-ray continuum into our line-of-sight. However, lack of the predicted absorption and/or emission features are a problem for this model unless the scatterer has a very high temperature.
4. A multicomponent description of the soft excess is the most physically reasonable one. We find that scattered flux plus 40% due to an ionized absorber is most consistent with the spectral (lack of strong features) and temporal (lack of strong variability) data. In addition, the Fe K edge energy is consistent with the energy predicted from this model.
5. Positive residuals between 1.5–3.0 keV, consistent with being Si recombination, are observed during the low flux state of the source. If the Si features are real, this is the first such detection in an AGN and their presence has implications for the interpretation of partial covering results obtained from proportional counter experiments.

It may be that the real test as to the origin of the soft excess in NGC 4151 will be in its variability pattern. It is also of critical importance to determine the spectrum of the spatially extended soft flux in NGC 4151. In addition, better signal-to-noise observations are necessary to search for weak spectral features at $<1.5$ keV energies. ASCA, now in orbit, can observe weak spectral features ($\sim 20$ eV EW at low energies) with 30,000 s integration times and should be able to detect features associated with a warm absorber as well as to allow a thorough testing of complex models for the soft excess.

H. N. thanks the NRC for a senior fellowship at NASA/GSFC and the US-Israel Binational Science Foundation for support through grant no. 89-00179. K. W. acknowledges the support of a NASA Graduate Researcher's Fellowship. This paper is the result of research toward the fulfillment of requirements of the Ph.D. degree at the University of Maryland. The authors would also like to thank the referee for many helpful comments.

## REFERENCES

Antonucci, R. R. J., & Miller, J. S. 1985, ApJ, 297, 621
Barr, P., White, N. E., Sanford, P. W., & Ives, J. C. 1977, MNRAS, 181, 43p
Clavel, J., et al. 1987, ApJ, 321, 251
Elvis, M., Briel, U. G., & Henry, J. P. 1983, ApJ, 268, 105
Elvis, M., Fassnacht, C., Wilson, A. S., & Briel, U. 1990, ApJ, 361, 459
Fiore, F., Elvis, M., Mathur, S., Wilkes, B. J., & McDowell, J. C. 1993, ApJ, 415, 129
Gursky, H., Kellogg, E. M., Leong, C., Tananbaum, H., & Giacconi, R. 1971, ApJ, 165, L43
Halpern, J. P. 1984, ApJ, 281, 90

Hamilton, A. J. S., Sarazin, C. L., & Szymkowiak, A. E. 1986, ApJ, 300, 713
Heckman, T. M., & Balick, B. 1983, ApJ, 268, 102
Holt, S. S., Mushotzky, R. F., Becker, R. H., Boldt, E. A., Serlemitsos, P. J., Szymkowiak, A. E., & White, N. E. 1980, ApJ, 241, L13
Jahoda, K., et al. 1992, in The X-Ray Background, ed. X. Barcons & A. C. Fabian (Cambridge Univ. Press), 240
Khachikian, E., & Weedman, D. W. 1974, ApJ, 192, 581
Kriss, G. A., et al. 1992, ApJ, 392, 485
Kriss, G., Evans, I., Ford, H., Tsvetanov, Z., Davidson, A., & Kinney, A. 1993, in The Nature of Compact Objects in AGN, ed. A. Robinson & R. J. Terlevich (Cambridge University Press), in press
Krolik, J. H., McKee, C. F., & Tartar, C. B. 1981, ApJ, 249, 422
Krolik, J. H., & Vrtilek, J. M. 1984, ApJ, 279, 521
Maisack, M., & Yaqoob, T. 1991, A&A, 249, 25
Makishima, K. 1986, in The Physics of Accretion onto Compact Objects, ed. K. O. Mason, M. G. Watson, & N. E. White (Berlin: Springer)
Maoz, D., et al. 1991, ApJ, 367, 493
Marshall, F. E., et al. 1993, ApJ, 405, 168
Miller, J. S., Goodrich, R. W., & Mathews, W. G. 1991, ApJ, 378, 47
Nandra, K., Pounds, K. A., Stewart, G. C., George, I. M., Hayashida, K., Makino, F., & Ohashi, T. 1991, MNRAS, 248, 760
Netzer, H. 1993, ApJ, 411, 594
Pan, H. C., Stewart, G. C., & Pounds, K. A. 1990, MNRAS, 242, 177
Pedlar, A., Howley, P., Axon, D. J., & Unger, S. W. 1992, MNRAS, 259, 369
Peréz-Fournon, I., & Wilson, A. S. 1990, ApJ, 356, 456
Perola, G. C., et al. 1986, ApJ, 306, 508
Perotti, F., et al. 1981, ApJ, 247, L63
Pounds, K. A., Warwick, R. S., Culhane, J. L., & de Korte, P. A. J. 1986, MNRAS, 218, 685
Raymond, J. C., & Smith, B. 1977, ApJS, 35, 419
Reichert, G. A., Mushotzky, R. F., & Holt, S. S. 1986, ApJ, 303, 87
Schmidt, G. D., & Miller, J. S. 1980, ApJ, 240, 759
Serlemitsos, P. J., et al. 1992, in Frontiers of X-Ray Astronomy, ed. Y. Tanaka & K. Koyama (Tokyo: Universal Academy), 221
Shafer, R. A., Haberl, F., & Arnaud, K. A. 1989, XSPEC: An X-ray Spectral Fitting Package, ESA TM-09 (Paris: ESA)
Simkin, S. M. 1975, ApJ, 200, 567
Turner, T. J., Done, C., Mushotzky, R., Madejski, G., & Kunieda, H. 1992, ApJ, 391, 102
Weaver, K. A. 1994, Ph.D. thesis, University of Maryland
Weaver, K. A., et al. 1992, ApJ, 401, L11 (Paper I)
———. 1994, ApJ, submitted
Yaqoob, T., & Warwick, R. S. 1991, MNRAS, 248, 773
Yaqoob, T., Warwick, R. S., & Pounds, K. A. 1989, MNRAS, 236, 153
Yaqoob, T., Warwick, R. S., Makino, F., Otani, Y., & Sokoloski, J. 1993, MNRAS, 262, 435